Water maintains the UV-Vis spectral features during the insertion of anionic Naproxen and Ibuprofen into model cell membranes

Natalia Rojas-Valencia,[*,†] Sara Gómez,[*,‡] Tommaso Giovannini,[‡] Chiara Cappelli,[‡] Albeiro Restrepo,[¶] and Francisco Núñez–Zarur[*,†]

†*Facultad de Ciencias Básicas, Universidad de Medellín, Carrera 87 No. 30-65, 050026, Medellín, Colombia*

‡*Scuola Normale Superiore, Classe di Scienze, Piazza dei Cavalieri 7, 56126, Pisa, Italy*

¶*Instituto de Química, Universidad de Antioquia UdeA, Calle 70 No. 52-21, Medellín, Colombia*

E-mail: nandrea.rojas@udea.edu.co; sara.gomezmaya@sns.it; fnunez@udemedellin.edu.co

Abstract

UV-Vis spectra of anionic Ibuprofen and Naproxen in a model lipid bilayer of the cell membrane are investigated using computational techniques in combination with a comparative analysis of drug spectra in purely aqueous environments. The simulations aim at elucidating the intricacies behind the negligible changes in the maximum absorption wavelength in the experimental spectra. A set of configurations of the systems constituted by lipid, water, and drugs or just water and drugs are obtained from classical Molecular Dynamics simulations and UV-Vis spectra are computed in the framework of atomistic Quantum Mechanical /Molecular Mechanics (QM/MM) approaches together with Time-Dependent Density Functional Theory (TD-DFT). Our results suggest that the molecular orbitals involved in the electronic transitions are the same regardless of the chemical environment. A thorough analysis of the contacts between the drug and water molecules reveals that no significant changes in UV-Vis spectra are a consequence of Ibuprofen and Naproxen molecules being permanently microsolvated by water molecules despite the presence of lipid molecules. Water molecules microsolvate the charged carboxylate group as expected but also microsolvate the aromatic regions of the drugs.

1 Introduction

Nonsteroidal anti-inflammatory drugs (NSAIDs) are a family of chemical compounds widely used worldwide to relieve pain, fever, and swelling.[1] According to their chemical structure they are mainly classified as salicylates, sulfonanilides, and derivatives of acetic acid, enolic acid, and propionic acid.[2] The latter category includes Ibuprofen, (IBU), [(RS)-2-(4-(2-methylpropyl)phenyl propanoic acid)] and Naproxe, (NAP), [(2S)-2-(6-methoxynaphthalen-2-yl) propanoic acid]. Ibuprofen is used to treat pain in rheumatoid disorders and inflammatory diseases,[3] whereas Naproxen is mostly employed in the treatment of acute arthritis, osteoarthritis, musculoskeletal pain inflammation, and dysmenorrhea,[4] and it is thought to have a longer duration of action.[5]

IBU and NAP are weak acids with pK_a values of 5.2 and 4.2, respectively,[6] and thus they are found as deprotonated species, IBU^- and NAP^-, at physiological pH values. Another common characteristic of these molecules is their amphiphilic character due to the presence of one acetate and aromatic groups connected by a bridging carbon that is a chiral center. The S-conformations (see Figure 1) are reported to have greater therapeutic action.[7,8]

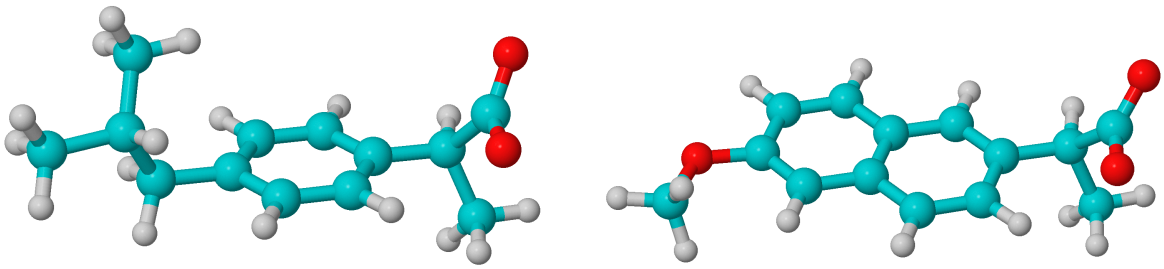

Figure 1: Isolated anionic forms of (S)–Ibuprofen (left) and (S)–Naproxen (right). Color code: C atoms in light blue, O atoms in red, and H atoms in light grey.

The main mechanism of action of IBU^- and NAP^-, as well as of the general set of NSAIDs, involves the inhibition of the cyclooxygenase (COX) enzyme during the production

of prostaglandins from the arachidonic acid.[9,10] Prostaglandins are mediators in the response of the body to a pathological or physiological stimulus.[9,11] In contrast to the NSAIDs therapeutic action, some experimental and computational studies suggest that they could affect cell membrane properties such as its fluidity and function due to their interaction with phospholipids which are the building blocks of the membrane.[2,12,13] Concerning those interactions, researchers have reached a consensus on the key role played by the NSAIDs lipid affinity in both the (undesired) toxic and therapeutic actions.[12]

The interaction between drugs and the lipidic environment of the cell membrane has been routinely investigated by means of the estimation of the drug partition coefficient in a system composed of octanol and water.[14] Notwithstanding, the complexity of the biological system is not well captured by this environment, and thus few reports have focused on more realistic models of cell membranes.[14–16] It is well known that the hydrophobic character of NSAIDs determines the extent to which they can be distributed in the membrane.[17] This fact has important implications for the lipid bilayer structure. For instance, Manrique-Moreno et al.[13,18] studied the effect of IBU^- and NAP^- on liposomes as model membranes under physiological conditions (pH 7.4). By using different experimental techniques such as Differential Scanning Calorimetry (DSC) and Fourier Transform Infrared Spectroscopy (FTIR), among others, the authors found changes both in the transition phase temperature and in the vibration of some polar groups of the lipid model when the drug was present. However, they did not find evidence of its insertion in the hydrophobic part of the membrane. Thereafter, several studies using Neutron Diffraction and Molecular Dynamics (MD) simulations were carried out to explore in more detail the location of the drug within the membrane.[19–21] Overall, those studies suggested that IBU and NAP can reside in the hydrophobic core and in the interface between the polar and nonpolar regions of the lipid bilayer in their protonated and deprotonated states, respectively. Without any exception, all the above studies agree that the anionic drug can produce changes in the lipid bilayer structure even though those drugs are not able to cross the membrane through a passive permeation mechanism. There-

fore, the simplistic view offered by the octanol/water partition coefficient is not good enough to gain reliable information on the insertion process. In the last two decades, experimental UV-Vis spectroscopy has been proposed as a new strategy to get the partition coefficient of drugs in lipid membranes due to the electronic changes of the molecule according to its chemical environment.[15,22]

Different experimental techniques have been used to get insight into the behavior of the complex tertiary systems constituted by phospholipids, drugs, and water. For the IBU^- and NAP^- cases, UV-Vis measurements have been performed in aqueous solutions and in lipid environments and the results did not show significant changes in the maximum absorption wavelength.[23,24] However, since the drug has interactions of a very distinct nature when is surrounded by water molecules or when immersed in a lipid environment, important band shifts should be expected as it happens when a generic solute is dissolved in polar *vs* in non-polar solvents.[25–27] To the best of our knowledge, no previous studies focus on understanding the intricacies involved in the electronic transitions of the drug as a response to the surrounding environment. Certainly, more detailed information about the system might be obtained using computational spectroscopy. In particular, the combination of MD simulations with Time-Dependent Density Functional Theory (TD-DFT) in the framework of Quantum Mechanics (QM)/Molecular Mechanics (MM) has proved to be a good strategy to study the absorption spectra of large-sized systems.[28–33]

In this work, we investigate, from a computational perspective, the reasons behind the small changes in experimental UV-Vis spectra of IBU^- and NAP^- when going from aqueous solution to the aqueous lipidic environment. To that end, we take reported configurations[21,34] from combined MD simulations performed with the umbrella sampling method[35] and calculate the electronic transitions involved in absorption spectra using QM/MM combined with TD-DFT. To account for the different chemical environments surrounding the drug,

the electronic transitions are characterized in a set of configurations belonging to the three key points where IBU^- or NAP^- could be located, namely, the aqueous environment, at the polar region of the lipid bilayer and at the polar/non–polar interface of the membrane, as pointed out in recent works.[21,34]

The paper is structured as follows: in the next section, to contextualize the problem, the results of the previously reported Gibbs free energy profiles for the insertion of IBU^- and NAP^- into model cell membranes are briefly summarized, thus explaining the key points from which the configurations are taken. Then, the computational details are given and in the section 3, UV-Vis and ECD spectra results are presented and discussed. Finally, in Section 4, some conclusions are drawn.

2 Methods

MD runs coupled with QM/MM have been shown to be particularly reliable because, on the one hand, MD simulations allow to capture the microscopic behavior of the molecules and have a good representation of macroscopic properties due to the ability of getting a set of different configurations of the equilibrated system, which on average represent the behavior of the system as a whole.[36–38] On the other hand, QM/MM approaches are relatively inexpensive because only a portion of the system to be excited is modeled at the QM level, while the environment is described classically with MM force fields.[39–42] By following such a computational strategy, it has been possible to get an outstanding reproduction of experimental UV-Vis spectra at reduced computational cost.[43–47] There are different conceptual ways of combining QM and MM parts, that differ from each other in the inclusion and method of describing the mutual interactions.[40,48,49] Possible approaches consist of Mechanical and Electrostatic Embedding. In the latter, the interaction term is formulated in terms of a set of fixed charges, whereas more sophisticated approaches make charges to adjust to the QM density,[40,50] however they may require specific parametrization for the considered environ-

ments.[27] For this reason, in this work, we exploit electrostatic embedding, which has proven to be efficient and accurate in other complex problems, for example, in the calculation of the UV-Vis spectra of the residue pairs having persistent contacts in the attaching of the SARS-CoV-2 (and its variants) to the ACE2.[51,52] Also, a non-polarizable QM/MM approach was followed by Cwiklik et al.[33] to study a system aiming at reproducing the experimental absorption and emission spectra of PRODAN into a lipid bilayer, without elucidating the nature of the absorption electronic transitions.

In the present work, we use a set of equilibrated configurations at 317 K reported in previous papers.[20,21] To summarize, during the MD simulations, each drug, anionic naproxen and ibuprofen, interacted with a lipid bilayer in an aqueous environment as a model of the cell membrane using the CHARMM36[53] and CHARMM General (CGenFF) force fields[54,55] for the lipid bilayer and for the drugs, respectively, allowing molecular conformational freedom. The lipid bilayer was constructed with 64 Dimyristoylphosphatidylcholine (DMPC) molecules per layer. Explicit TIP3P water molecules were also included in the simulation box. A free energy profile for the affinity of the drug in different lipidic environments of the system was obtained following a reaction coordinate, running from the center of the bilayer to the aqueous environment. Three critical points were identified along the reaction coordinate: 1) a local minimum when the drug resides in the aqueous environment, 2) a maximum of the barrier when the drug is facing the polar part of the lipid, which is characterized by Choline and phospholipids groups and 3) the global minimum of the free energy when the drug is located in the interface between the polar/non-polar part of the lipids. These key points for IBU^- and NAP^- are displayed in Figure 2 along with a comparison of the free energy curves. It is worth mentioning that the global minima also represent the equilibrium position of the drugs and are in agreement with reported experimental results. More details about those studies can be found elsewhere.[20,21]

Based on the three critical points of the Gibbs free energy mentioned above (aqueous

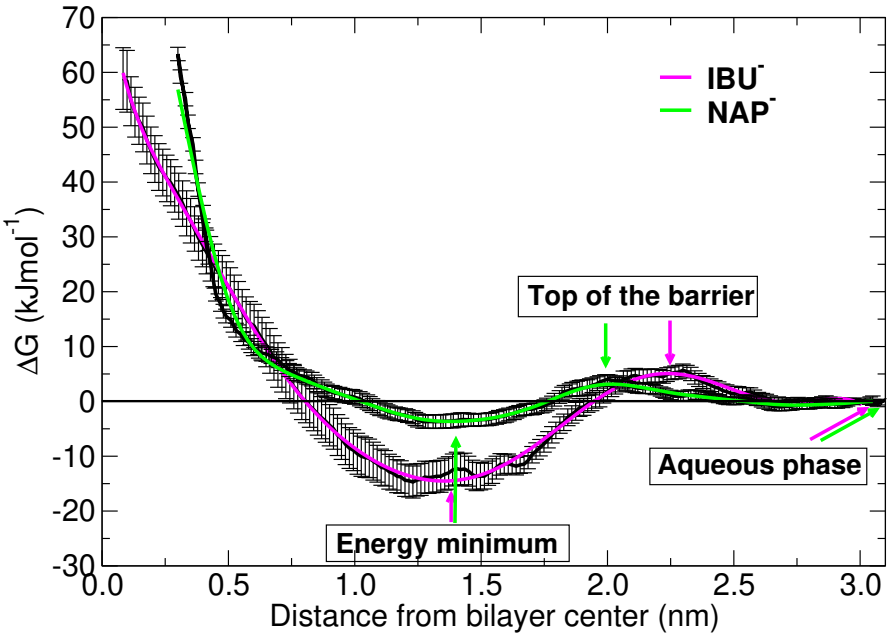

Figure 2: Free energy profiles for the insertion processes of the drugs into model dimyristoylphosphatidylcholine (DMPC) membranes at 317 K. The equilibrium position[20,21] is reached at ≈ 1.35 nm from the center of the lipid bilayer for both anions. Image adapted from Ref. 20. Copyright 2018 Royal Society of Chemistry, and from Ref. 21. Copyright 2021 American Chemical Society.

phase, top of the barrier, and energy minimum), we selected 200 random snapshots from the last 7 ns and 15 ns of the production steps of the reported MD simulations for each one of the three different chemical environments. In an effort to reduce the size of the system while maintaining an accurate representation of the chemical environment during the simulation, only the water molecules within a cut-off radius of 3.6 Å from each atom of the drug were considered in the aqueous environment. Expanding the cut-off radius to 5.0, 10.0 and 15.0 Å for a chosen configuration did not change the results as shown in Figure S1 in the Supporting Information, SI. 15.0 Å was the threshold for including lipids and water at the top of the barrier and in the energy minimum. A random snapshot of each point is shown in Figure 3 and the cut regions are highlighted. To determine the cut-off radius, we employed information from former studies[21,34] where radial distribution functions (RDFs) were exploited to define the boundaries and calculate quantum mechanical properties of the system –electron densities, natural charges, Non-covalent Interactions (NCI), Natural Bond

Orbitals (NBOs)– in order to study the intermolecular interactions[56–58] taking place between the drug and the environment (water and phospholipids). As opposed to other works,[21,34] here, the first hydration sphere of the nonpolar part of the drug (first maximum of RDF) was explicitly considered, thus increasing the size of the regions. Finally, for the top of the barrier and the energy minimum, the coordinate corresponding to the emergence of a plateau in the RDF was chosen as the last solvation sphere. Entire phospholipids are always included if present.

Non-polarizable, electrostatic embedding QM/MM calculations were performed to obtain the electronic absorption spectra. The first ten excited states were taken into account in each case and were enough to reproduce experimental findings. As a first approach, the drug (IBU^- or NAP^-) was included in the QM portion, whereas the remaining system was described through an electrostatic embedding using the same fixed charges employed during the MD runs. For two arbitrarily chosen configurations in the aqueous phase and at the energy minimum, all neighbors within 2.0 and 2.5 Å (2.5 and 3.5 Å at the energy minimum) were also included in the QM region. No significant differences in the results obtained by enlarging the QM region are reported (see Figure S2 in the SI), thus suggesting that solute-environment electrostatic interactions dominate over polarization and non-electrostatics (in this case only Pauli repulsion and Charge Transfer) for the selected systems. Vertical transition energies were computed for each configuration by means of TD-DFT calculations at the CAM-B3LYP/6-311++g(d,p) level of theory. This model chemistry has been chosen for two reasons: after benchmarking, (see Figure S3 in the SI) it showed the best reproduction of experimental UV-Vis absorption spectra when an anionic ibuprofen molecule was embedded by an aqueous environment, represented with the polarizable continuum model (PCM). Additionally, other studies with similar systems also used the same level of theory with a good reproduction of spectral properties.[59] Further analysis employing mechanical instead of electrostatic embedding yielded poor reproduction of the experimental data as can be seen in Figure S4 in the SI.

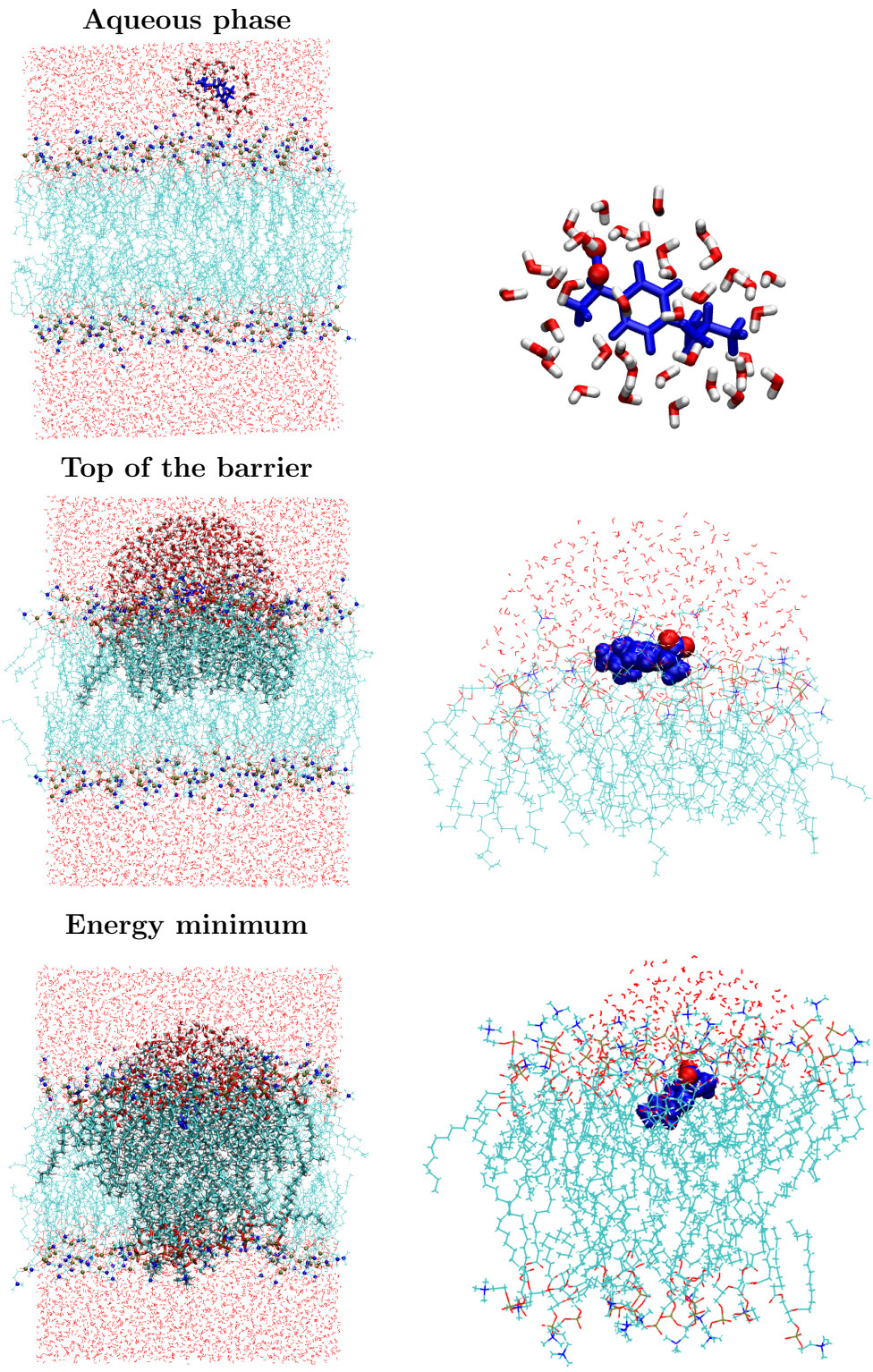

Figure 3: Representation of the selected system in the different environments: aqueous phase (top), top of the barrier (middle), and energy minimum (bottom). The highlighted regions in the left column, which are enlarged in the right column, correspond with the cut-off radius taken into account to calculate the UV-Vis spectra.

The obtained spectroscopic information was then convoluted using Gaussian functions with a full width half maximum (FWHM) of 0.4 eV to carry out a proper comparison between simulated and experimental absorption spectra. Despite using a large number of snapshots (600 in total, 200 in each environment) the spectra converged after considering only 140 snapshots (see Figure S5 in the SI). We also characterized all electronic transitions in terms of Canonical Molecular Orbitals (CMO) as described in the NBO framework.

All calculations were performed using the Gaussian 16 package.[60] NBO7[61] was employed for the CMO calculations.

3 Results and Discussion

In this section, the simulated UV-Vis absorption and ECD spectra of both Ibuprofen and Naproxen in three different chemical environments of the NSAID/DMPC/water system (aqueous phase, top of the barrier, and energy minimum) are presented. First, the results for the drugs in aqueous solution are analyzed and then the findings for each drug in an aqueous lipidic environment are shown. Later, an analysis of the small spectral differences is carried out.

3.1 UV-Vis spectra of ibuprofen and naproxen

3.1.1 Drugs in aqueous environments

The reported experimental UV-Vis spectrum of ibuprofen in aqueous environment has two absorption maxima at 222 and 190 nm.[24,62] As a matter of fact, it has been claimed that excitation energies occurring at wavelengths below 200 nm are difficult to interpret if the measure is not taken in *vacuum*.[63] For this reason, we will be focused on the 200-300 nm range. Experimental spectral features of naproxen in aqueous environment involve two bands,

one in the 210-250 nm interval, centered at ≈ 230 nm, with a small shoulder in the vicinity of 270 nm, and a broad second band going from 300 to 340 nm.[23,64] These bands are usually associated to $\pi \rightarrow \pi^*$ transitions.[65] Figure 4 shows the QM/MM UV-Vis absorption spectra obtained from the convolution of a total of 200 snapshots when the drug is surrounded only by water molecules. Both simulated spectra (bottom panel of Figure 4) match the most important spectral characteristics observed in the experiments, with solvated IBU^- having an exceptional agreement. For solvated NAP^-, although the most intense band appears slightly shifted from the experimental position, the shoulder and the low-intensity band are mixed in a single spread band that covers all the region above 260 nm. Our computations are fully consistent with other measurements which do not distinguish the low-intensity band from its onset.[66] These results confirm the accuracy of the level of theory used in this work.

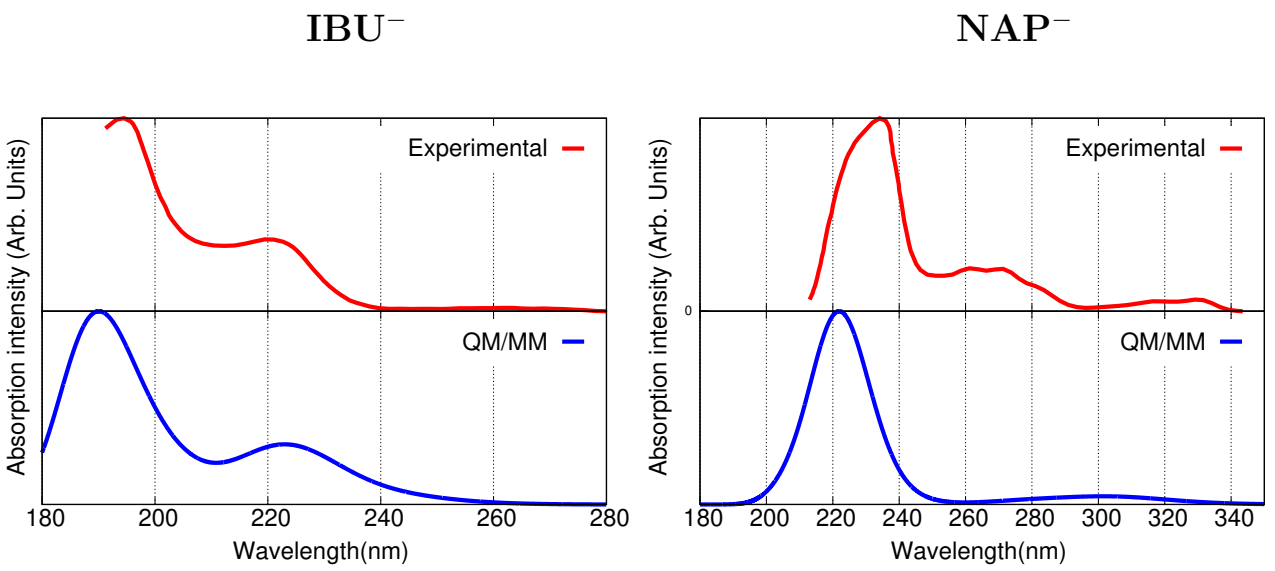

Figure 4: Experimental[23,24] (top) and simulated QM/MM CAM-B3LYP/6-311++g(d,p)/Electrostatic Embedding (bottom) UV-Vis spectra of IBU^- (left) and NAP^- (right) in aqueous solution. 200 snapshots were considered in the calculations. Averaged spectra were convoluted with an FWHM of 0.4 eV and normalized to the highest intensity band.

3.1.2 Drugs in aqueous lipidic environment

As mentioned in the Introduction and as shown in Figure 5, there is a negligible difference of about 2 nm for IBU^- (blue shifted) and no difference for NAP^- in the experimental maximum wavelength when the surrounding environment of the drug is changed from purely aqueous to lipidic.[24] Figure 5 also compares the calculated and experimental spectra. The computed spectra including the sticks in the three different chemical environments, namely, aqueous solution, top of the barrier, and energy minimum (see Figures 2 and 3), are displayed in Figure 6 for both drugs. Notice in Table S1 of the SI that the 0.6 and 1.5 nm red shifts for the calculated aqueous and water/drug/membrane spectra are within the standard deviations. It is evident that beyond the different absolute intensities, there are no significant changes in the spectroscopic information related to the position of the main bands. Such an analogous behavior in diverse environments has been reported by Cwiklik et al.[33] who studied the changes in the absorption spectra for the insertion of PRODAN into palmitoyloleoylphosphatidylcholine (POPC) bilayers and pointed out a relatively weak or almost imperceptible dependence of the absorption energy on the type of environment.

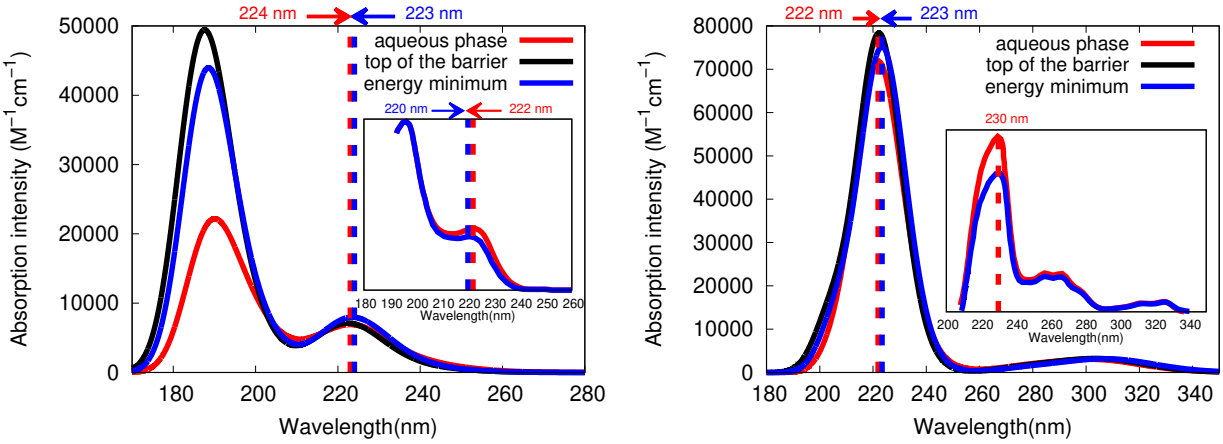

Figure 5: Simulated and experimental (insets) UV–Vis spectra for Ibuprofen (left) and Naproxen (right) in the three studied environments. Vertical lines mark the exact positions of the absorption maxima.

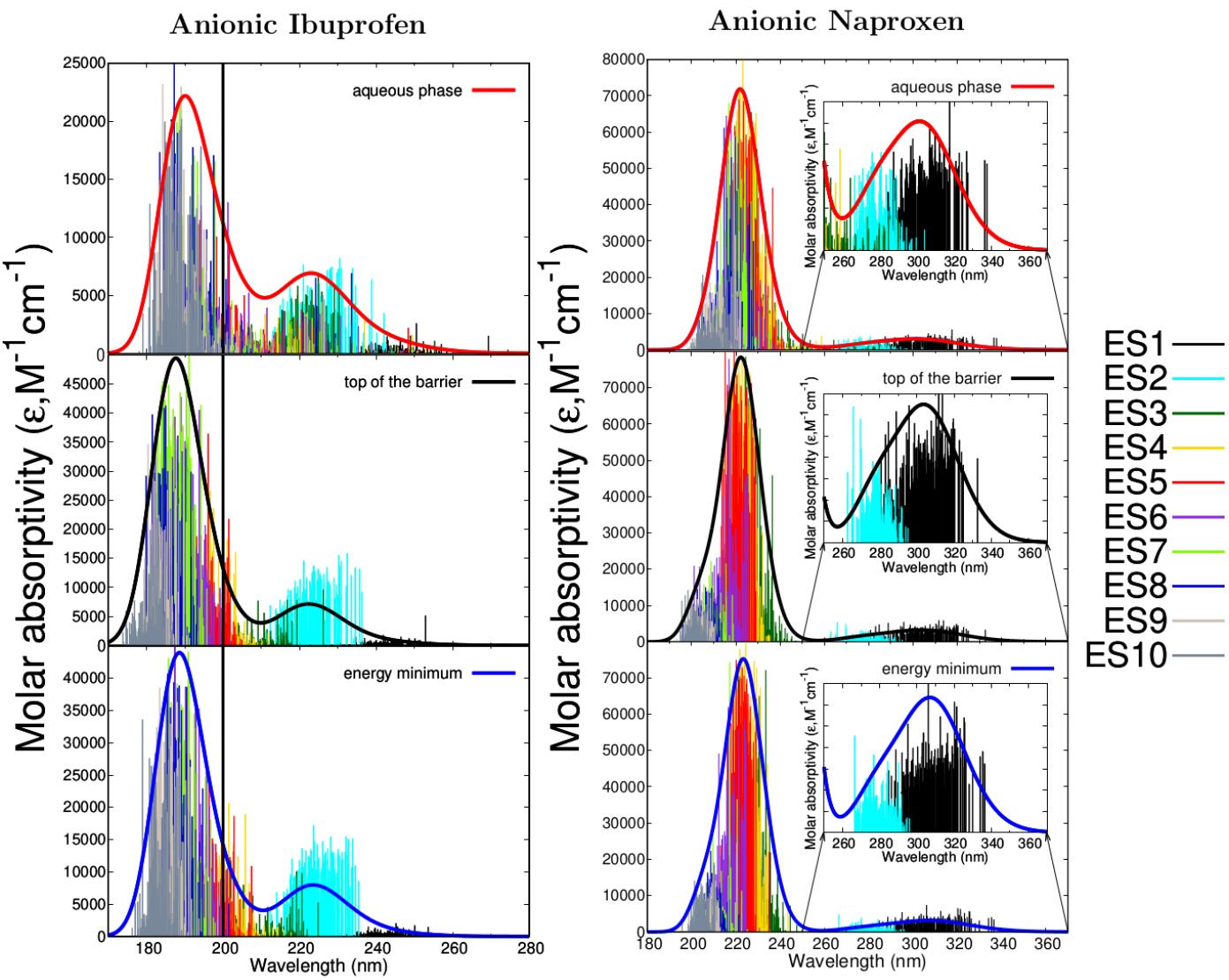

Figure 6: Stick-like UV-Vis spectra of Ibuprofen (left) and Naproxen (right) in the three different chemical environments considered in this work (see Figure 3). The shape of the convoluted spectrum is shown as a solid line. Each type of transition is color-coded, e. g., Excited state 1 (ES1) in black and Excited state 2 (ES2) in cyan. The vertical solid lines in the IBU$^-$ case, mark the boundary up to the highest resolved experimental information. An inset showing the structure of the low-intensity band is also provided for NAP$^-$.

Figure 6 reports the stick-like spectra of embedded IBU$^-$ and NAP$^-$ in all environments. It means that the raw data extracted from QM/MM calculations on each snapshot are reported as a position/oscillator strengths spectrum, which gives insight into the natural spreading of the transition bands, both in wavelengths and intensities. In addition, each

stick is colored depending on the associated transition (see labels at the right of the figure). In the IBU^- case, it is interesting to notice that for both the top of the barrier and the energy minimum, the band at 222 nm results from a single electronic transition to the excited state 2 (ES2). Conversely, in aqueous environment, although the major contribution comes from ES2, there are other electronic transitions leading to the appearance of such a band. These electronic transitions can be appreciated by taking a look at the diversity in the stick colors making part of the most intense absorption band (see Figure 6, top panel).

For NAP^-, the presence of the two fused aromatic rings makes the absorption spectra very distinct with respect to its ibuprofen counterpart which has only one ring. This structural feature has been documented to displace the position of the absorption maxima to longer wavelengths as in the benzene→naphthalene→anthracene series.[67] As displayed in the inset of the right panel of Figure 6, the first low-intensity band (between 250 and 340 nm) is basically made up of two transitions, i.e. ES1 (black color) and ES2 (cyan color). Additionally, the most intense band in NAP^- (240 nm) which comprises several excited states may overlap with the 222 nm band in IBU^- when IBU^-/NAP^- mixtures are considered, making it difficult to assign specific electronic transitions. For both anions in aqueous phase, these two bands, which are combinations of different electronic excited states, have a more spread distribution with respect to the other two environments. This observation may be attributed to the higher mobility of the drug in water solution, as compared to the limited freedom provided by the lipidic environment. Further evidence to support this point is obtained from the standard deviations listed in Table S1 in the SI.

A deeper insight into the nature of the absorption bands can be attained by looking at the molecular orbitals (MOs) involved in the electronic transitions. IBU^- MOs in the three considered environments are depicted in Figure 7 along with their corresponding contributions to ES2. Table S2 in the SI lists the same information for the lowest-energy excited

state ES1. It can be observed that regardless of the environment, the excitation involves the HOMO and the first unoccupied MOs (LUMO, LUMO+1, LUMO+2, or LUMO+3 orbitals). Thus, the ES2 transition can be expressed as HOMO $\rightarrow$ 0.84(LUMO+1) + 0.55(LUMO+3), HOMO $\rightarrow$ LUMO and HOMO $\rightarrow$ 0.78LUMO + 0.62(LUMO+2) transitions for the drug into the aqueous phase, top of the barrier and energy minimum, respectively.

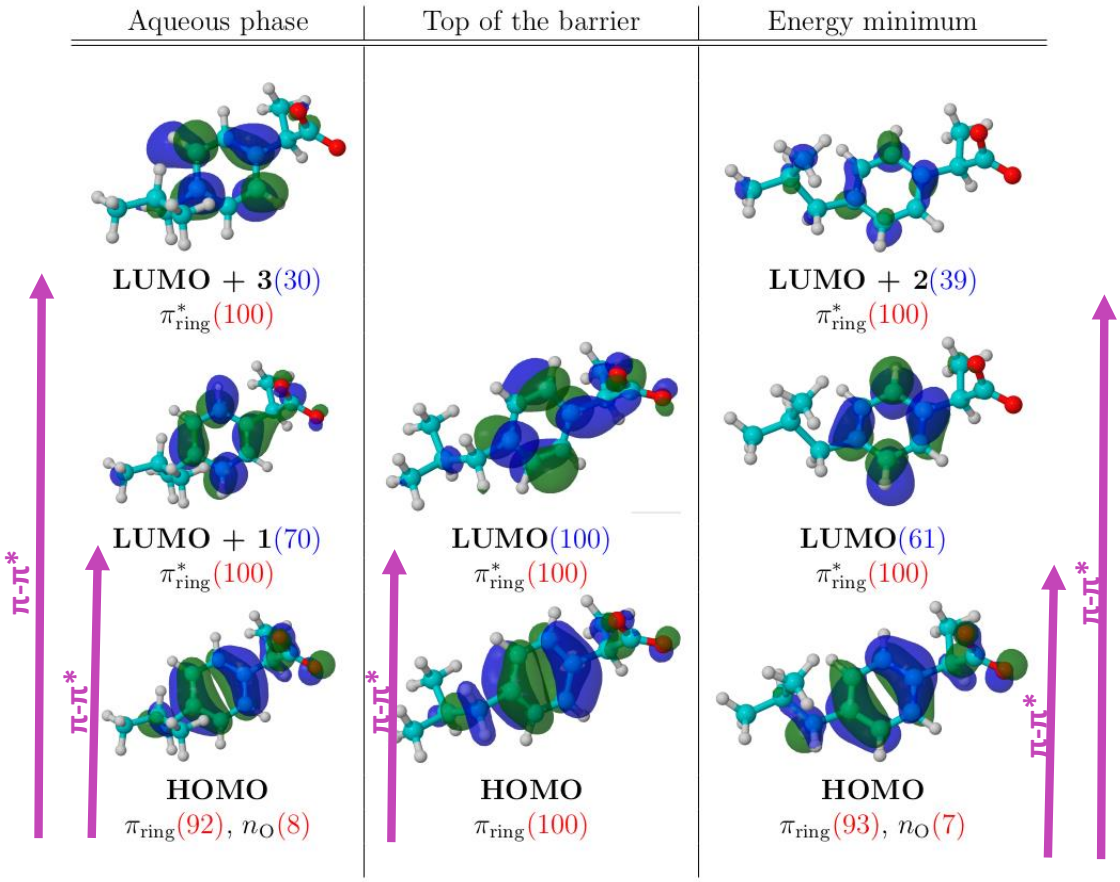

Figure 7: MOs involved in the electronic transition to ES2, responsible for the experimentally observed band of anionic Ibuprofen in different environments (see Figure 6, left panel). Blue and red numbers in parentheses correspond to the contributions of the MOs to the electronic transition and the contributions of the NBOs to the MOs after the CMO decomposition, respectively. Isosurface value: 0.03. These results correspond to a randomly chosen snapshot.

In addition, each MO can be characterized with the tools provided by NBO, specifically,

the Localized Analysis of CMOs, which allows for the assignment of the transition from/to specific portions of the chromophore. For instance, it is clearly seen that for IBU^-, the highest contributions to the HOMO orbitals come from both π bonds of the aromatic ring and from the lone pairs of the oxygen atoms always with a higher percentage of π_{ring}, independently of the environment. Furthermore, all unoccupied orbitals involve only π^* orbitals from the aromatic ring, validating the $\pi \rightarrow \pi^*$ assignment documented in the literature for the absorption band with a maximum at 222 nm when the drug is surrounded by aqueous environment.[59]

From the MO perspective, the NAP^- case is much more complex. Table S3 in the SI lists the orbitals having the largest coefficient for each electronic transition in one randomly chosen snapshot. It is important to stress that although we are showing results for one snapshot only, those findings are representative of the average of the electronic transitions for the entire group of configurations. The MOs involved in the ES1 and ES2 of NAP^- (giving rise to the band at 340 nm) are HOMO and HOMO-1. HOMO-1 has contributions of π orbitals from the aromatic ring and from the oxygen of the carboxylic group. Contributions from the ether oxygen are viewed in the case of the HOMO. Instead, excited states from ES3 to ES10 (leading to the highest intensity band) encompass an assorted set of occupied orbitals. Oscillator strengths in Table S3 in the SI indicate that ES5 and ES8 for aqueous phase, ES3 and ES4 for the top of the barrier, and ES4 and ES6 for energy minimum, are the primary excited states giving rise to the absorption intensities. Notice also that regardless of the environment, unoccupied orbitals (LUMO, LUMO+1,...) often involve the π^* from the aromatic rings. Several MOs involved in electronic transitions are displayed in Figure S6 as well as their CMO decomposition, which reinforces the $\pi \rightarrow \pi^*$ assignment link to that band.

It is worth mentioning that an implicit description of aqueous phase by means of PCM model yields similar MOs (and their contributions) as those obtained by using the atomistic

QM/MM approach. However, PCM cannot be exploited to describe the lipidic environment because a dielectric constant is not able to fairly represent the more complex top of the barrier and energy minimum environments. Thus, this highlights the need of using an atomistic QM/MM simulation when investigating electronic properties of large systems.

3.1.3 A short note on the electronic circular dichroism (ECD) spectra of anionic ibuprofen and naproxen

Chiroptical properties are particularly sensitive to the solute-environment interactions and to the instantaneous configuration of the system.[68] Further analysis of changes in the electronic structure of both drugs was done by calculating the ECD spectra. In Figure 8, the experimental (top) and convoluted (bottom) spectra for the drugs in aqueous environment are shown, exhibiting good agreement with the experimental positive and negative patterns for IBU^- and NAP^-, respectively. Simulated ECD spectra in the three critical points of the free energies profiles (see Figure 2) are included in Figure S7 in the SI and, as in the case of the UV-Vis spectra, there are no significant changes in the spectral curves in the different chemical environments.

For the particular case of naproxen, it has been revealed that the (R)- and (S) enantiomers had an unusual inversion in their ECD signals in the presence of ethanol and water when compared with polar aprotic solvents such as acetonitrile.[66] If we consider that this change in sign is only given by the polarity of the environment, the fact of maintaining the same ECD signs in our computational spectra suggests that there is not much change in the chemical environment as the drug goes from the aqueous phase to its location at the energy minimum, in the polar/non-polar interphase of the lipid bilayer.

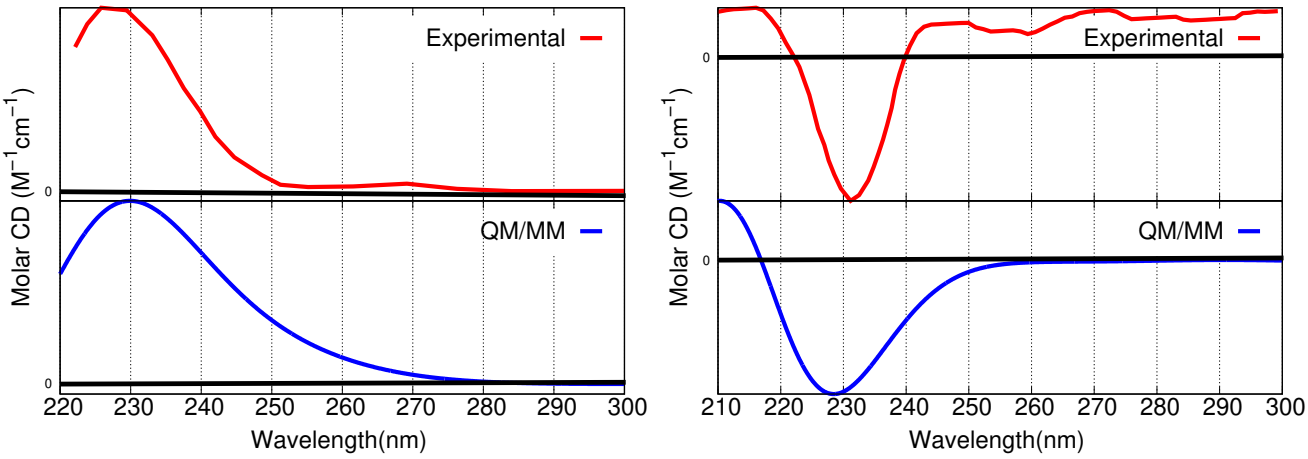

Figure 8: Experimental[66,69] (top) and simulated QM/MM CAM-B3LYP/6-311++g(d,p)/Electrostatic Embedding (bottom) Electronic Circular Dichroism spectra of IBU^- (left) and NAP^- (right) in aqueous solution. 200 snapshots were considered in the calculations. Averaged spectra were convoluted with an FWHM of 0.4 eV and normalized for comparison purposes.

Being clear that ECD properties of IBU^- and NAP^- do not depend on the environment, nor do their electronic absorption spectra, perhaps another spectroscopy like excited state emission spectra could be more fruitful to assess the insertion processes in cell membranes. Regarding emission spectra, for PRODAN in a membrane-type environment, a significant influence of the environment was observed in both experiments and simulations, in contrast to the weak dependence seen in the absorption processes.[33]

3.2 Analysis of spectral differences between all environments

From the above description of UV-Vis and ECD spectra, we have established a good agreement between experimental and calculated spectra for both drugs when they are embedded in diverse environments. From those results, it is clear the similarity between the UV-Vis and ECD spectra in the three regions, supported by almost the same molecular orbitals involved in the electronic transitions. Another piece of evidence to be added to that puzzling

situation is that there is no inversion of the ECD sign when polarity changes (as opposed to what was reported in Ref. 66). In order to give an answer to the key question of why there are no differences across the spectra in the several critical points of the free energy profile, it is necessary to analyze what is happening around the drug in its different locations in the system.

This fact can be explored by relying on the information reported in the works of Rojas-Valencia et al.,[21,34] In the first place, the authors analyzed the distribution of water molecules in the immediate vicinity (within 3.0 Å) of the entire drug and pointed out that no matter the environment, there are at least ten water molecules surrounding either IBU^- or NAP^-. Variations in the total number of drug-water interactions as a function of the distance from the bilayer center are collected in the left panel of Figure 9. Since our orbital analysis indicated that as a general rule the π orbitals are the most heavily involved ones in the electronic transitions, we went deeper and discriminate how many of those waters around the molecule were located close to the rings. The number of contacts between the solvent and the aromatic portion of each drug is plotted in the right panel of Figure 9. As expected, the majority of water molecules are placed near the carboxylate group because the formal charge is a strong attractor during the insertion process. Indeed, the microsolvation of IBU^- with up to three water molecules has been already studied[70] and it was clear that solvent molecules in direct contact with anionic Ibuprofen, preferred to cluster around the carboxylate oxygen atoms forming cyclic or bridged charge-assisted hydrogen bond networks. Here, we noticed that there are also persistent stabilizing interactions between the drug ring(s) and a few water molecules, about five and six for IBU^- or NAP^-, respectively. Therefore, it seems that the drug's local environment is quite similar in the three key points while it travels to the inner part of the bilayer, even if the global environment dictated by the presence or absence of lipids is changing.

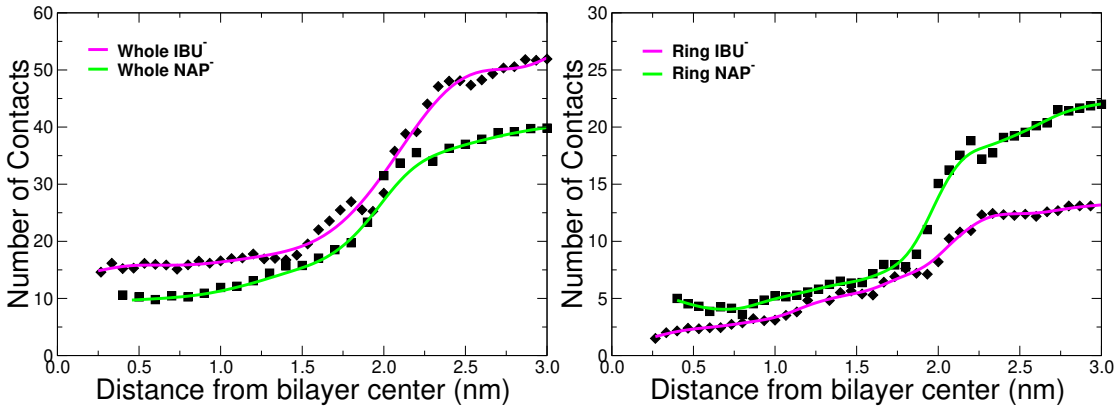

Figure 9: Number of water molecules within 3.0 Å of any given atom (left) or a specific atom of the ring(s) (right) in Naproxen and Ibuprofen during their insertion into the lipid bilayer.

Second, in Refs. 21,34, the same authors computed the NCI surfaces between the drug and its surroundings and found that there are many tiny collective non-covalent interactions throughout its insertion, with no significant qualitative changes. In fact, several of those interactions are associated with the ring$\cdots$solvent contacts mentioned above. These two aspects highlight the idea that the chemical environment around the NSAIDs stays approximately the same along its path from the aqueous environment up to the bottom of the energy profile. This translates into weak changes in the electronic structure reflected in turn in no large differences seen in the UV-Vis and ECD spectra.

4 Conclusions

We have applied a multiscale QM/MM approach based on electrostatic embedding to simulate the UV-Vis absorption and ECD spectra of anionic naproxen and ibuprofen during their individual travel to the inner part of the cell membrane, by means of a series of TDDFT calculations. Spectra were calculated in three key points of the Gibbs free energy profile, namely, the aqueous phase, the top of the barrier, and the energy minimum, sampling configurations from MD trajectories previously reported. Having many accessible configurations leads to the arising of a natural broadening in the spectra. As a result of the application

of this methodology, all calculated spectra exhibit very good agreement when compared against available experimental data, being able to reproduce the main spectral features and the non-significant changes reported when the drug's spectra were measured in different environments. In all cases, electronic transitions were analyzed in terms of the orbitals involved. The CMO decomposition supports the $\pi \rightarrow \pi^*$ transitions assigned to the main bands. Our analysis of the excited states and orbitals, complemented by the quantification of the number of contacts between the drug and the solvent molecules along the insertion, allows us to gain insight into the origin of the small or almost imperceptible differences in both electronic absorption and circular dichroism spectra. In particular, we show that regardless of the environment there are always water molecules in the immediate vicinity of the ring/aromatic portion of IBU^- and NAP^-, thus maintaining similar local surroundings and not affecting to a large extent the electronic properties of these two compounds. Our calculations also indicate that the choice of the DFT functional and type of embedding were important steps, having large impacts on the accuracy of the results obtained. Finally, our findings are encouraging for using these methodologies when studying complex systems like drugs in lipidic environments and to understand where and how these or other spectroscopies could be eventually useful to distinguish between insertion or intercalation phenomena. In this respect, fluorescence has been proven to be useful in the case of other complex systems[33] and will be investigated in future works.

Acknowledgement

NRV thanks the Ministerio de Ciencias y Tecnología de Colombia, MINCIENCIAS, for a postdoctoral fellowship. FNZ acknowledges Universidad de Medellín for continuous support. Internal support from Universidad de Antioquia via "Estrategia para la sostenibilidad" is also acknowledged. We gratefully acknowledge the Center for High Performance Computing (CHPC) at SNS for providing the computational infrastructure.

Supporting Information Available

Plots for the analysis of the level of theory, the convergence of the UV-Vis spectra according to the number of snapshots, and the UV-Vis and ECD spectra for the three phases considered in this work. Tables including the main molecular orbitals involved in the ES1 for ibuprofen and all transitions for Naproxen. The oscillator strength values for naproxen in all environments were also included. Figure representing the most important MOs involved in the electronic transitions of naproxen in the three phases.

References

(1) Ghlichloo, I.; Gerriets, V. *Nonsteroidal anti-inflammatory drugs (NSAIDs)*; StatPearls Publishing, Treasure Island (FL), 2022.

(2) Pereira-Leite, C.; Nunes, C.; Reis, S. Interaction of nonsteroidal anti-inflammatory drugs with membranes: in vitro assessment and relevance for their biological actions. *Prog. Lipid Res* **2013**, *52*, 571–584.

(3) Ngo, V. T. H.; Bajaj, T. *Ibuprofen*; StatPearls Publishing, Treasure Island (FL), 2022.

(4) Brutzkus, J. C.; Shahrokhi, M.; Varacallo, M. *Naproxen*; StatPearls Publishing, Treasure Island (FL), 2022.

(5) Schiff, M.; Minic, M. Comparison of the analgesic efficacy and safety of nonprescription doses of naproxen sodium and Ibuprofen in the treatment of osteoarthritis of the knee. *J. Rheumatol.* **2004**, *31*, 1373–1383.

(6) Barbato, F.; La Rotonda, M. I.; Quaglia, F. Interactions of nonsteroidal antiinflammatory drugs with phospholipids: comparison between octanol/buffer partition coefficients and chromatographic indexes on immobilized artificial membranes. *J. Pharm. Sci.* **1997**, *86*, 225–229.

(7) Evans, A. M. Comparative pharmacology of S (+)-ibuprofen and (RS)-ibuprofen. *Clin. Rheumatol.* **2001**, *20*, 9–14.

(8) Kean, W. F.; Lock, C. J.; Rischke, J.; Butt, R.; Buchanan, W. W.; Howard-Lock, H. Effect of R and S enantiomers of naproxen on aggregation and thromboxane production in human platelets. *J. Pharm. Sci.* **1989**, *78*, 324–327.

(9) Vane, J.; Botting, R. Anti-inflammatory drugs and their mechanism of action. *Inflamm. Res.* **1998**, *47*, 78–87.

(10) Duggan, K. C.; Walters, M. J.; Musee, J.; Harp, J. M.; Kiefer, J. R.; Oates, J. A.; Marnett, L. J. Molecular basis for cyclooxygenase inhibition by the non-steroidal anti-inflammatory drug naproxen. *J. Biol. Chem.* **2010**, *285*, 34950–34959.

(11) Goodwin, G. *Prostaglandins: Biochemistry, Functions, Types, and Roles*; Cell biology research progress; Nova Science Publisher, New York, USA, 2010.

(12) Tsuchiya, H.; Mizogami, M. Membrane interactivity of non-steroidal anti-inflammatory drugs: a literature review. *J. Adv. Med. Biomed. Res.* **2020**, *31*, 1–30.

(13) Manrique-Moreno, M.; Villena, F.; Sotomayor, C. P.; Edwards, A. M.; Muñoz, M. A.; Garidel, P.; Suwalsky, M. Human cells and cell membrane molecular models are affected in vitro by the nonsteroidal anti-inflammatory drug ibuprofen. *Biochim. Biophys. Acta - Biomembr.* **2011**, *1808*, 2656–2664.

(14) Seydel, J.; Wiese, M.; Mannhold, R.; Kubinyi, H.; Folkers, G. *Drug-Membrane Interactions: Analysis, Drug Distribution, Modeling*; Methods & Principles in Medicinal Chemistry; Wiley, 2009.

(15) Magalhães, L. M.; Nunes, C.; Lúcio, M.; Segundo, M. A.; Reis, S.; Lima, J. L. High-throughput microplate assay for the determination of drug partition coefficients. *Nat. Protoc.* **2010**, *5*, 1823–1830.

(16) Bennion, B. J.; Be, N. A.; McNerney, M. W.; Lao, V.; Carlson, E. M.; Valdez, C. A.; Malfatti, M. A.; Enright, H. A.; Nguyen, T. H.; Lightstone, F. C., et al. Predicting a drug's membrane permeability: A computational model validated with in vitro permeability assay data. *J. Phys. Chem. B* **2017**, *121*, 5228–5237.

(17) Lichtenberger, L. M.; Zhou, Y.; Jayaraman, V.; Doyen, J. R.; O'Neil, R. G.; Dial, E. J.; Volk, D. E.; Gorenstein, D. G.; Boggara, M. B.; Krishnamoorti, R. Insight into NSAID-induced membrane alterations, pathogenesis and therapeutics: characterization of interaction of NSAIDs with phosphatidylcholine. *Biochim. Biophys. Acta - Mol. Cell Biol. Lipids* **2012**, *1821*, 994–1002.

(18) Manrique-Moreno, M.; Garidel, P.; Suwalsky, M.; Howe, J.; Brandenburg, K. The membrane-activity of Ibuprofen, Diclofenac, and Naproxen: A physico-chemical study with lecithin phospholipids. *Biochim. Biophys. Acta - Biomembr.* **2009**, *1788*, 1296–1303.

(19) Boggara, M. B.; Mihailescu, M.; Krishnamoorti, R. Structural association of nonsteroidal anti-inflammatory drugs with lipid membranes. *J. Am. Chem. Soc.* **2012**, *134*, 19669–19676.

(20) Rojas-Valencia, N.; Lans, I.; Manrique-Moreno, M.; Hadad, C. Z.; Restrepo, A. Entropy drives the insertion of ibuprofen into model membranes. *Phys. Chem. Chem. Phys.* **2018**, *20*, 24869–24876.

(21) Rojas-Valencia, N.; Gómez, S.; Núñez-Zarur, F.; Cappelli, C.; Hadad, C.; Restrepo, A. Thermodynamics and Intermolecular Interactions during the Insertion of Anionic Naproxen into Model Cell Membranes. *J. Phys. Chem. B* **2021**, *125*, 10383–10391.

(22) Santos, N. C.; Prieto, M.; Castanho, M. A. Quantifying molecular partition into model systems of biomembranes: an emphasis on optical spectroscopic methods. *Biochim. Biophys. Acta - Biomembr.* **2003**, *1612*, 123–135.

(23) Fernandes, E.; Soares, T. B.; Gonçalves, H.; Lúcio, M. Spectroscopic studies as a toolbox for biophysical and chemical characterization of lipid-based nanotherapeutics. *Front. Chem.* **2018**, *6*, 323.

(24) Du, L.; Liu, X.; Huang, W.; Wang, E. A study on the interaction between ibuprofen and bilayer lipid membrane. *Electrochim. Acta* **2006**, *51*, 5754–5760.

(25) Raab, M. T.; Prỳmek, A. K.; Giordano, A. N. Estimation of the ground and excited state dipole moments for ibuprofen and naproxen sodium using the solvatochromic shift method. *J. Undergrad. Chem. Res.* **2021**, *20*, 68.

(26) Chen, X.; Qiao, W.; Miao, W.; Zhang, Y.; Mu, X.; Wang, J. the Dependence of implicit Solvent Model parameters and electronic Absorption Spectra and photoinduced charge transfer. *Sci. Rep.* **2020**, *10*, 1–8.

(27) Ambrosetti, M.; Skoko, S.; Giovannini, T.; Cappelli, C. Quantum Mechanics/Fluctuating Charge Protocol to Compute Solvatochromic Shifts. *J. Chem. Theory Comput.* **2021**, *17*, 7146–7156.

(28) Brunk, E.; Rothlisberger, U. Mixed quantum mechanical/molecular mechanical molecular dynamics simulations of biological systems in ground and electronically excited states. *Chem. Rev.* **2015**, *115*, 6217–6263.

(29) Zhang, K.; Ren, S.; Caricato, M. Multistate QM/QM Extrapolation of UV/Vis Absorption Spectra with Point Charge Embedding. *J. Chem. Theory Comput.* **2020**, *16*, 4361–4372.

(30) Zuehlsdorff, T. J.; Isborn, C. M. Modeling absorption spectra of molecules in solution. *Int. J. Quantum Chem.* **2019**, *119*, e25719.

(31) Giovannini, T.; Macchiagodena, M.; Ambrosetti, M.; Puglisi, A.; Lafiosca, P.; Lo Gerfo, G.; Egidi, F.; Cappelli, C. Simulating vertical excitation energies of sol-

vated dyes: From continuum to polarizable discrete modeling. *Int. J. Quantum Chem.* **2019**, *119*, e25684.

(32) Goletto, L.; Giovannini, T.; Folkestad, S. D.; Koch, H. Combining multilevel Hartree–Fock and multilevel coupled cluster approaches with molecular mechanics: a study of electronic excitations in solutions. *Phys. Chem. Chem. Phys.* **2021**, *23*, 4413–4425.

(33) Cwiklik, L.; Aquino, A. J.; Vazdar, M.; Jurkiewicz, P.; Pittner, J.; Hof, M.; Lischka, H. Absorption and fluorescence of PRODAN in phospholipid bilayers: a combined quantum mechanics and classical molecular dynamics study. *J. Phys. Chem. A* **2011**, *115*, 11428–11437.

(34) Rojas-Valencia, N.; Gómez, S.; Montillo, S.; Manrique-Moreno, M.; Cappelli, C.; Hadad, C.; Restrepo, A. Evolution of Bonding during the Insertion of Anionic Ibuprofen into Model Cell Membranes. *J. Phys. Chem. B* **2020**, *124*, 79–90.

(35) Kästner, J. Umbrella sampling. *Wiley Interdiscip. Rev. Comput. Mol. Sci.* **2011**, *1*, 932–942.

(36) Skoko, S.; Ambrosetti, M.; Giovannini, T.; Cappelli, C. Simulating Absorption Spectra of Flavonoids in Aqueous Solution: A Polarizable QM/MM Study. *Molecules* **2020**, *25*, 5853.

(37) Giovannini, T.; Grazioli, L.; Ambrosetti, M.; Cappelli, C. Calculation of ir spectra with a fully polarizable qm/mm approach based on fluctuating charges and fluctuating dipoles. *J. Chem. Theory Comput.* **2019**, *15*, 5495–5507.

(38) Giovannini, T.; Ambrosetti, M.; Cappelli, C. A polarizable embedding approach to second harmonic generation (SHG) of molecular systems in aqueous solutions. *Theor. Chem. Acc.* **2018**, *137*, 74.

(39) Senn, H. M.; Thiel, W. QM/MM methods for biomolecular systems. *Angew. Chem. Int. Ed.* **2009**, *48*, 1198–1229.

(40) Giovannini, T.; Egidi, F.; Cappelli, C. Molecular spectroscopy of aqueous solutions: a theoretical perspective. *Chem. Soc. Rev.* **2020**, *49*, 5664–5677.

(41) Gómez, S.; Bottari, C.; Egidi, F.; Giovannini, T.; Rossi, B.; Cappelli, C. Amide Spectral Fingerprints are Hydrogen Bonding-Mediated. *J. Phys. Chem. Lett* **2022**, *13*, 6200–6207.

(42) Dohn, A. O. Multiscale electrostatic embedding simulations for modeling structure and dynamics of molecules in solution: a tutorial review. *Int. J. Quantum Chem.* **2020**, *120*, e26343.

(43) Gómez, S.; Giovannini, T.; Cappelli, C. Multiple Facets of Modeling Electronic Absorption Spectra of Systems in Solution. *ACS Physical Chemistry Au* **2023**, *3*, 1–16.

(44) Gómez, S.; Giovannini, T.; Cappelli, C. Absorption spectra of xanthines in aqueous solution: A computational study. *Phys. Chem. Chem. Phys.* **2020**, *22*, 5929–5941.

(45) Gómez, S.; Egidi, F.; Puglisi, A.; Giovannini, T.; Rossi, B.; Cappelli, C. Unlocking the power of resonance Raman spectroscopy: The case of amides in aqueous solution. *J. Mol. Liq.* **2022**, *346*, 117841.

(46) Uribe, L.; Gómez, S.; Giovannini, T.; Egidi, F.; Restrepo, A. An efficient and robust procedure to calculate absorption spectra of aqueous charged species applied to NO_2^-. *Phys. Chem. Chem. Phys.* **2021**, *23*, 14857–14872.

(47) Uribe, L.; Gómez, S.; Egidi, F.; Giovannini, T.; Restrepo, A. Computational hints for the simultaneous spectroscopic detection of common contaminants in water. *J. Mol. Liq.* **2022**, *355*, 118908.

(48) Warshel, A.; Levitt, M. Theoretical studies of enzymic reactions: dielectric, electrostatic and steric stabilization of the carbonium ion in the reaction of lysozyme. *J. Mol. Biol.* **1976**, *103*, 227–249.

(49) Mennucci, B.; Corni, S. Multiscale modelling of photoinduced processes in composite systems. *Nat. Rev. Chem.* **2019**, *3*, 315–330.

(50) Cappelli, C. Integrated QM/polarizable MM/continuum approaches to model chiroptical properties of strongly interacting solute–solvent systems. *Int. J. Quantum Chem.* **2016**, *116*, 1532–1542.

(51) Gómez, S. A.; Rojas-Valencia, N.; Gómez, S.; Egidi, F.; Cappelli, C.; Restrepo, A. Binding of SARS-CoV-2 to Cell Receptors: A Tale of Molecular Evolution. *ChemBioChem* **2021**, *22*, 724–732.

(52) Gómez, S. A.; Rojas-Valencia, N.; Gómez, S.; Cappelli, C.; Restrepo, A. The Role of Spike Protein Mutations in the Infectious Power of SARS-COV-2 Variants: A Molecular Interaction Perspective. *ChemBioChem* **2022**, *23*, e202100393.

(53) Klauda, J. B.; Venable, R. M.; Freites, J. A.; O'Connor, J. W.; Tobias, D. J.; Mondragon-Ramirez, C.; Vorobyov, I.; MacKerell, A. D.; Pastor, R. W. Update of the CHARMM All-Atom Additive Force Field for Lipids: Validation on Six Lipid Types. *J. Phys. Chem. B* **2010**, *114*, 7830–7843, PMID: 20496934.

(54) Vanommeslaeghe, K.; MacKerell, A. D. Automation of the CHARMM General Force Field (CGenFF) I: Bond Perception and Atom Typing. *J. Chem. Inf. Model* **2012**, *52*, 3144–3154.

(55) Vanommeslaeghe, K.; Raman, E. P.; MacKerell, A. D. Automation of the CHARMM General Force Field (CGenFF) II: Assignment of Bonded Parameters and Partial Atomic Charges. *J. Chem. Inf. Model* **2012**, *52*, 3155–3168.

(56) Gómez, S.; Rojas-Valencia, N.; Gómez, S. A.; Cappelli, C.; Merino, G.; Restrepo, A. A molecular twist on hydrophobicity. *Chem. Sci.* **2021**, *12*, 9233–9245.

(57) Rojas-Valencia, N.; Gómez, S.; Guerra, D.; Restrepo, A. A detailed look at the bonding interactions in the microsolvation of monoatomic cations. *Phys. Chem. Chem. Phys.* **2020**, *22*, 13049–13061.

(58) Gómez, S. A.; Rojas-Valencia, N.; Gómez, S.; Lans, I.; Restrepo, A. Initial recognition and attachment of the Zika virus to host cells: A molecular dynamics and quantum interaction approach. *ChemBioChem* **2022**, e202200351.

(59) Gómez, S.; Rojas-Valencia, N.; Giovannini, T.; Restrepo, A.; Cappelli, C. Ring Vibrations to Sense Anionic Ibuprofen in Aqueous Solution as Revealed by Resonance Raman. *Molecules* **2022**, *27*, 442.

(60) Frisch, M. J.; Trucks, G. W.; Schlegel, H. B.; Scuseria, G. E.; Robb, M. A.; Cheeseman, J. R.; Scalmani, G.; Barone, V.; Petersson, G. A.; Nakatsuji, H. et al. Gaussian 16 Revision B.01. 2016; Gaussian Inc. Wallingford CT.

(61) Glendening, E. D.; Badenhoop, J. K.; Reed, A. E.; Carpenter, J. E.; Bohmann, J. A.; Morales, C. M.; Karafiloglou, P.; Landis, C. R.; Weinhold, F. NBO 7.0. 2018; Theoretical Chemistry Institute, University of Wisconsin, Madison, WI.

(62) Choina, J.; Kosslick, H.; Fischer, C.; Flechsig, G.-U.; Frunza, L.; Schulz, A. Photocatalytic decomposition of pharmaceutical ibuprofen pollutions in water over titania catalyst. *Appl. Catal. B: Environ* **2013**, *129*, 589 – 598.

(63) Picollo, M.; Aceto, M.; Vitorino, T. UV-Vis spectroscopy. *Phys. Sci. Rev.* **2019**, *4*.

(64) Arany, E.; Szabó, R. K.; Apáti, L.; Alapi, T.; Ilisz, I.; Mazellier, P.; Dombi, A.; Gajda-Schrantz, K. Degradation of naproxen by UV, VUV photolysis and their combination. *J. Hazard. Mater.* **2013**, *262*, 151–157.

(65) Saji, R. S.; Prasana, J. C.; Muthu, S.; George, J.; Kuruvilla, T. K.; Raajaraman, B. Spectroscopic and quantum computational study on naproxen sodium. *Spectrochim. Acta - A: Mol. Biomol. Spectrosc.* **2020**, *226*, 117614.

(66) Ximenes, V. F.; Morgon, N. H.; Robinson de Souza, A. Solvent-dependent inversion of circular dichroism signal in naproxen: An unusual effect! *Chirality* **2018**, *30*, 1049–1053.

(67) Friedel, R.; Orchin, M. *Ultraviolet Spectra of Aromatic Compounds*; John Wiley & Sons, Inc., New York, 1951.

(68) Giovannini, T.; Egidi, F.; Cappelli, C. Theory and algorithms for chiroptical properties and spectroscopies of aqueous systems. *Phys. Chem. Chem. Phys.* **2020**, *22*, 22864–22879.

(69) Liu, M.; Chen, L.; Tian, T.; Zhang, Z.; Li, X. Identification and quantitation of enantiomers by capillary electrophoresis and circular dichroism independent of single enantiomer standard. *Anal. Chem.* **2019**, *91*, 13803–13809.

(70) Zapata-Escobar, A.; Manrique-Moreno, M.; Guerra, D.; Hadad, C. Z.; Restrepo, A. A combined experimental and computational study of the molecular interactions between anionic ibuprofen and water. *J. Chem. Phys.* **2014**, *140*, 184312.

TOC Graphic

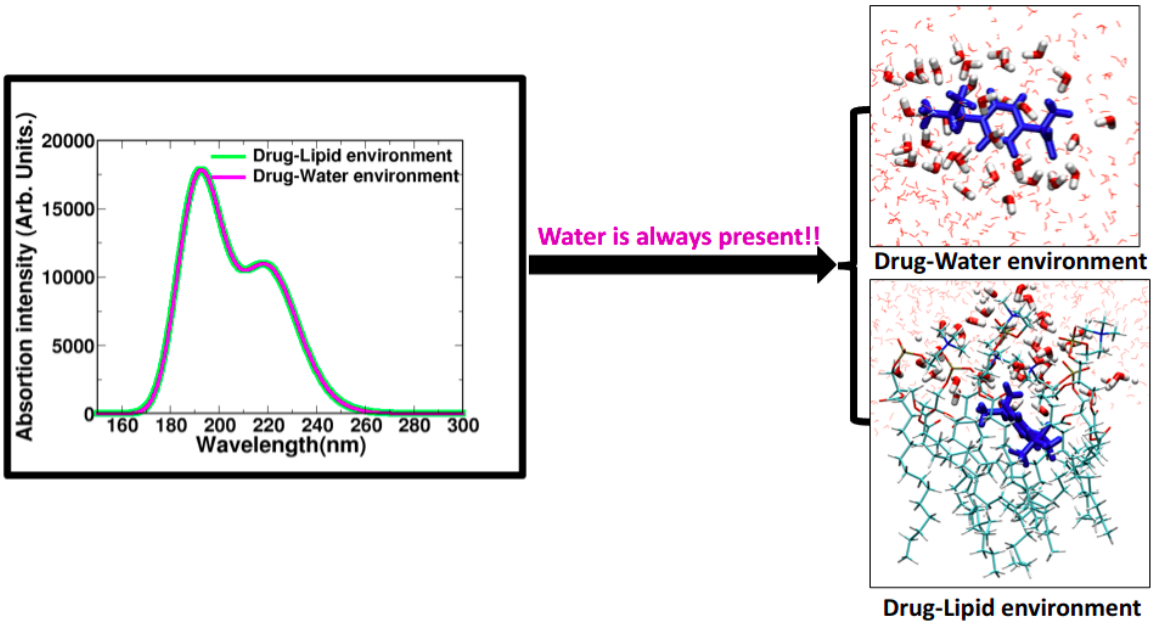
Absorption intensity (Arb. Units.)
20000
15000
10000
5000
0
160 180 200 220 240 260 280 300
Wavelength(nm)
Drug-Lipid environment
Drug-Water environment
Water is always present!!
Drug-Water environment
Drug-Lipid environment